Theoretical Study of the Site-Dependent Stabilities of Intrinsic Defects in a Polar BN Nanotube with Finite Length

ARTICLE *in* THE JOURNAL OF PHYSICAL CHEMISTRY C · NOVEMBER 2008

Impact Factor: 4.77 · DOI: 10.1021/jp806530n

3 AUTHORS, INCLUDING:

Gaoyang Gou
Xi'an Jiaotong University
15 PUBLICATIONS **293** CITATIONS

Theoretical Study of the Site-Dependent Stabilities of Intrinsic Defects in a Polar BN Nanotube with Finite Length

G. Y. Gou,[†] B. C. Pan,*[,†,‡] and L. Shi*[,†]

Hefei National Laboratory for Physical Science at Microscale, and Department of Physics, University of Science and Technology of China, Hefei 230026, P. R. China

Received: July 23, 2008; Revised Manuscript Received: October 6, 2008

Intrinsic defects, including single vacancy and Stone−Wales defects in a finite-length (8, 0) BN tube are investigated using density functional theory calculations. It is found that the stabilities of all defects are enhanced as they get close to the tube ends. We propose the possible physical origins for the defect energetic preference toward the tube ends and prove that the spontaneous electric polarization field of the BN tube can affect the stability of the defect by making the different electrostatic potential to the defect at different site. We also discuss the potential experimental consequences and provide the theoretical support for one experimental method for the synthesis of BN tubes.

1. Introduction

Boron nitride nanotubes (BNNTs), one of the representative one-dimensional III−V compounds structurally analogous to carbon nanotubes (CNTs), have attracted considerable interests ever since their discovery.[1,2] Unlike the metallic or semiconducting CNTs, BNNTs are semiconductors with a band gap width of about 5.8 eV,[3] almost independent of tube chirality and morphology.[4] Besides, BNNTs have excellent mechanical properties, thermal conductivity, and resistance to oxidation at high temperatures.[5−8] These exciting properties allow BNNTs to be complementary materials to CNTs, or even to replace CNTs for the possible application as nanoscale optical and electronic devices.

However, research works performed on BNNTs are lag far behind compared to those on CNTs. This is primarily as a result of the difficulties involved in BNNTs preparation.[9] Therefore, a better understanding about the growth mechanism of BNNTs is an important issue. Recently, Arenal et al.[10] have proposed a root-growth mechanism for the single-walled BNNTs prepared by laser vaporization technique, based on vapor−liquid−solid (VLS) model. However, different boron-based compounds and other impurities were identified in their raw synthesized products. How to get rid of these defects and synthesize the highly purified BNNT samples, one critical issue related to the growth mechanism, is still unclear.

To provide the possible solution to such a problem theoretically, we may borrow the ideas from the theoretical model on CNTs given by Ding.[11] In his paper, the author proved that defects in a finite-length CNT can diffuse to the tube open end, where they can be healed under a "scooter" mechanism. For BNNT, the following issues need to be investigated: (i) Will the stabilities of defects in a finite-length BNNT get enhanced as defects get close to tube ends? (ii) If so, what are the origins for the defect energetic preference toward the tube ends? It is noted that, despite the structural similarities, BNNTs do differ a lot from CNTs. For example, different behaviors of vacancies and SW defects between BNNTs and CNTs are found,[12−14] and there exist unique activation energies and reaction paths for diffusion and nucleation of vacancy defects in hexagonal BN system.[15] Moreover, BNNTs can exhibit piezoelectric properties[16] because of the heteropolar B−N bond. In this case, will the spontaneous polarization field of a polar BNNT affect the stability of defect on the tube? From this point of view, a theoretical investigation on the stability of defect at different site in a polar BN tube with finite length is of great necessity.

In this paper the site-dependent stabilities of intrinsic defects (single vacancy and Stone−Wales (SW) defects) in a finite-length BN tube have been investigated using ab inito calculations. It is found that stabilities of all defects studied are enhanced as they get close to the tube ends. The physical origins behind the site-dependent stabilities of defects are explored and the related experimental consequences are also discussed.

2. Theoretical and Computational Details

In this work, a segment of (8, 0) BNNT, which consists of four times of primary unit cell along the axial direction, is employed to represent a finite-length BN tube. As shown in Figure 1a, the BN tube is 17.95 Å in length, containing 64 B atoms and 64 N atoms. The two ends are made up of B and N atom rings respectively, and the dangling bonds are saturated by 16 H atoms. A vacuum region of 30 Å is used to separate the tube ends along the axial direction.

Three kinds of intrinsic defect, including single B and N atom vacancies (V_B and V_N) and SW defects, are under investigation. All these defects are created at the different sites along the tube axis to study their stabilities as a function of their distances to their nearest tube ends.

Formation energy is used to evaluate the stability of a defective system, which is defined as

$$E_{form} = E_{binding}[\text{defective}] - E_{binding}[\text{ideal}]$$
$$E_{binding} = E_{total} - n_B\mu_B - n_N\mu_N - n_H\mu_H \quad (1)$$

where E_{total} and $E_{binding}$ are total energy and binding energy of a given system. The chemical potentials, μ_B, μ_N, and μ_H are obtained by calculating the atomic energy of α-rhombohedral

* To whom correspondence should be addressed. E-mail: bcpan@ustc.edu.cn (B.C.P.); shil@ustc.edu.cn (L.S.).
† Hefei National Laboratory for Physical Science at Microscale.
‡ Department of Physics.

10.1021/jp806530n CCC: $40.75
Published on Web 11/14/2008

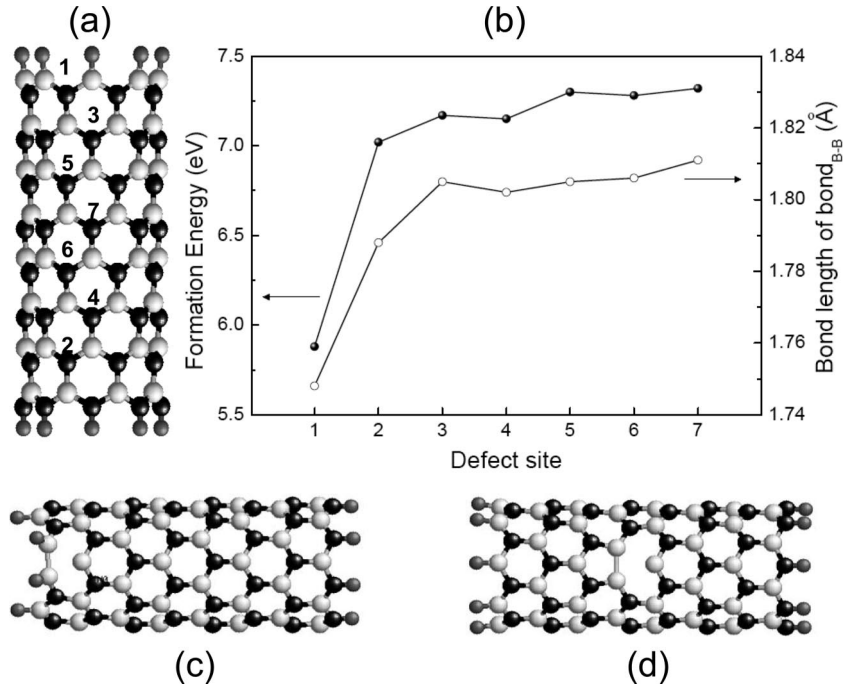

Figure 1. (a) Perfect (8, 0) BNNT, 1−7 indicate the sites where each N atom will be removed respectively. (b) The formation energy and bond length of B−B bond for the V_N defect at each site. (c and d) The optimized structures where a N atom is removed from sites 1 and 7, respectively. B, N, and H atoms are represented as white, black, and gray balls, respectively.

B,[17] N_2, and H_2 molecular. A positive E_{form} denotes the endothermal procedure for the formation of a defect.

Using the SIESTA code,[18−20] we carry out the structural optimization and total energy calculation within the spin-polarized density functional theory. The norm-conserving pseudopotentials generated using the Troullier−Martins scheme,[21] with atomic core and nonlocal components expressed in the fully separable form developed by Kleiman and Bylander,[22,23] are used to represent the valence electrons. Sankey finite-range pseudo atomic orbitals (PAOs)[25] are utilized as the split-valence double- ζ basis set (DZ) for the valence electrons of B, N, and H atoms. The generalized gradient approximation (GGA) in form of Perdew−Burke−Ernzerhof (PBE)[24] is adopted for exchange-correlation potential. The conjugate gradient (CG) algorithm[26] is adopted to fully relax the structures until the residual force acting on each atom is no more than 0.04 eV/Å.

3. Results and Discussion

3.1. Single Atom Vacancy Defects. A single B or N atom vacancy (V_B and V_N) can be formed by removing either a B or N atom from a perfect BNNT. After structural relaxation, V_N defect transforms into a 5−1DB configuration spontaneously. However, V_B with 3 dangling-bonds (3DBs) is formed initially, which is a metastable state. The stable V_B structure can be achieved through rebonding two of the DB atoms, and the final structure also characterizes a 5−1DB configuration.[27] In this way, both single vacancy defects exhibit one pentagon and one dangling bond (5−1DB) geometries around the local defect regions.

As shown in panel a of Figures 1 and 2, one of the N or B atoms marked with 1−7 in a perfect (8, 0) BNNT is removed respectively to form a V_N or V_B defect. These defects are characterized with different distances to their nearest tube ends. Figure 1, panels c and d, depicts the optimized configurations after one N atom is removed from site 1 and 7. It is found that the local structures of V_N defects at different sites are not significantly altered from each other. However, the situation for V_B defect gets complex since a vacancy with 3DBs is obtained initially. The possible stable V_B structures can be achieved in two ways: forming a homoatomic N−N bond either perpendicular or tilted to the tube axis.[28] In order to obtain the most stable V_B configurations corresponding to each sites, systematic relaxations of all possible V_B structures have been performed. Calculations indicate that except for the V_B defect at site 1 (displayed in Figure 2c), where the newly formed N−N bond is tilted to the tube axis, stable V_B defects at other sites all characterize the same 5−1DB structure (as shown in Figure 2d), with the N−N bonds perpendicular to the axis.

The relative formation energies corresponding to the optimal V_N and V_B defects at different sites are shown in panel b of Figures 1 and 2. It is clear that formation energies decrease (ΔE_{form} =1.5 eV for V_N and 1.9 eV for V_B) as the vacancies get closer to their nearest tube ends, indicating the enhancement of the defect stability.

Furthermore, we also investigate the change of local geometries around the single vacancy defects. For this purpose, the bond lengths of homoatomic bonds in single vacancies have been employed as the geometric parameters. The bond lengths of B−B or N−N bonds for V_N and V_B defects at different sites are displayed in panel b of Figures 1 and 2, respectively. It is found that the change of stabilities of single vacancy defects can be well correlated to their local geometry evolution. Similar to our previous work,[27] this kind of correlation originates from the bonding nature of the single vacancy defect. For the tube containing a single vacancy, the original sp^2 bonding character is distorted by $\sigma-\pi$ rehybridization, due to the presence of a dangling bond and formation of a new homoatomic bond.[29] Therefore, the stronger the rehybridization between $\sigma-\pi$ states, the more enhancement of homoatomic bond strength, and thus the single vacancy defect becomes more stable. For a finite-length tube, atoms at the ends fail to maintain the original lattice network, resulting in the elongation of the B−N bond near the ends and making σ and π bonds less rigid. So when an atom

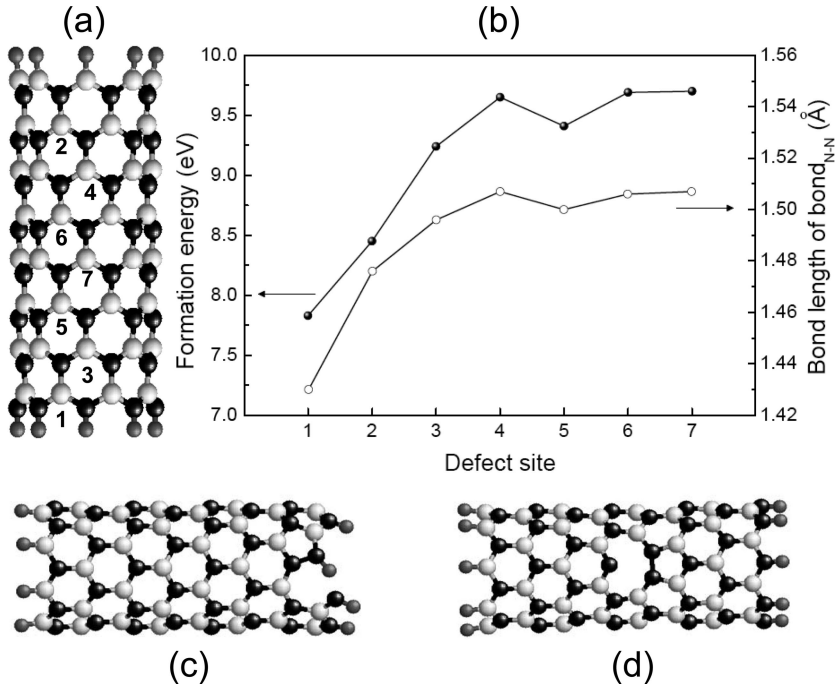

Figure 2. (a) Perfect (8, 0) BNNT, 1−7 indicate the sites where each B atom will be removed, respectively. (b) The formation energy and bond length of N−N bond for the V_B defect at each site. (c and d) The optimized structures where a B atom is removed from sites 1 and 7, respectively.

near the tube ends is removed, the σ and π states are more reactive to rehybridize and the corresponding vacancy is more stable. From this point of view, it is easily understood why the decrease of formation energy and bond length mainly occur for the single vacancies near the tube ends (vacancies at sites 1 and 2), as it is displayed in panel b of Figures 1 and 2.

To gain deep insight into single vacancy defects, their electronic structures are investigated. The density of states (DOS) for V_N and V_B at site 7 are displayed in Figure 3, panels a and b, respectively. Compared with a perfect BNNT, there exist additional states within the gap region in the case of defective BNNT containing a single vacancy, and the band gap is reduced effectively. Moreover, because of the unpaired electrons induced by the dangling bond, vacancy defects have the spin-splitting gap states.

When we extend our investigation to DOS of vacancies at different sites, it is found that the evolution of stability and local geometry of single vacancies also reflect on the change of their electronic structures. As the single vacancies move from B atom ring end to N end, the Fermi energy levels (E_F) of the corresponding systems are changing regularly. Figure 3, panels c and d, plots the E_F of V_N and V_B as a function of the defect axial positions. Interestingly, it is found that, except for the defects near the tube ends (at site 1 and 2), E_F for single vacancies at sites 3−7 exhibit linear variation as a function of their axial positions. Furthermore, it is also found that the HOMO−LUMO gaps of the vacancies near the tube ends increase significantly, reflecting the enhancement of homoatomic bond strength of the defect system.

3.2. Stone−Wales Defects. A SW defect is formed by rotating a B−N bond in the hexagonal network by $\pi/2$, resulting a pentagon−heptagon pair (5−7−7−5).[13] There are two nonequivalent B−N bonds in a BN tube, corresponding to two kinds of SW defects. As plotted in Figure 4d, a SW-I defect is generated by rotating an axial B−N bond by $\pi/2$, and a SW-II defect (shown in Figure 4e) is obtained by rotating a B−N bond tilted to the tube axis.

Based on the structural feature of (8, 0) BNNT, seven SW-I defects are created by rotating B−N bonds marked as 1, 3, 5, and 7, and six SW-II are formed through rotating bonds marked as 2, 4, and 6 (Figure 4a). The B−N bonds with the equal distance to their nearest tube ends are marked with the same number. In this way, we have created a series of SW defects on the tube surface, from one end to the other.

The stable SW defects are obtained after structural optimization. Optimal SW-I or SW-II defects at different sites exhibit similar pentagon−heptagon pair structures. Their relative formation energies are displayed in Figure 4b. It is found that SW-I defects are characterized with smaller formation energies compared to SW-II. Similar to single vacancy defects, the formation energies of SW defects also decrease ($\Delta E_{form} = 0.6$ eV for SW-I and 0.5 eV for SW-II) as the defects approach their nearest tube ends. Besides this general tendency, a small difference in the formation energy of SW defect is found. For the defects with the equal distance to their nearest tube ends, SW-I defects near the end consisting of B atom rings are more stable than the corresponding defects near the N end, whereas SW-II defects exhibit the opposite preference. When the defects are closer to their nearest ends, the larger formation energy differences will be made.

SW defects in BNNTs are likely to form when tubes are under large external tension. Formation of such a defect helps to release the strain induced by external tension and modifies the topological structure of the tube to some extent.[13] Thus, a conclusive understanding about the stability of SW defects should be based on its modification on the tube topological structure. For this purpose, the bond length deviation Δl is employed to evaluate how a SW defect affects the tube network. Here $\Delta l = \bar{l} - \bar{l}_0$, where $\bar{l}_0$ and $\bar{l}$ are the average bond length of B−N bonds in a perfect (8, 0) BNNT and B−N bonds around the SW defect region (indicated as gray area in Figure 4, panels d and e), respectively. The bond length deviations for the SW defects at different sites are displayed in Figure 4c. It is found that the SW-I defect has a positive bond length deviation,

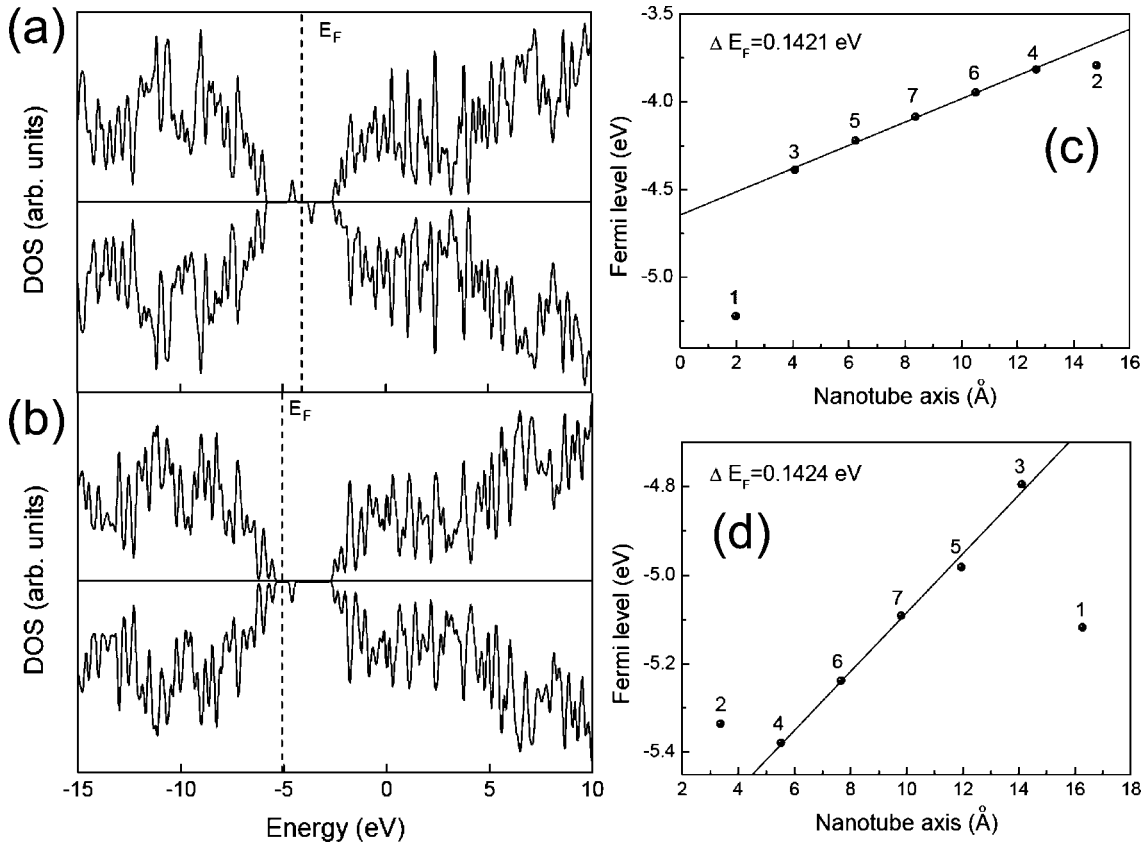

Figure 3. Density of states (DOS) for the BNNT with (a) V_N and (b) V_B defects. Two defects are obtained by removing a N or B atom from site 7, respectively. The DOS for majority-spin are plotted upward and minority-spin downward. Fermi energy levels (E_F) are represented as dotted lines. Fermi levels for the system with (c) V_N and (d) V_B defects as a function of the defect axial position. Solid lines are fitted to guide eyes.

whereas SW-II exhibits a negative deviation, which is similar to the SW defects in CNTs.[30]

Strikingly, both SW defects show the following site dependent evolutions: the smaller the absolute value of the bond length deviation, the lower defect formation energy. This finding seems to be in contradiction with the results in periodic defective tubes:[27,30] as the tube radius increases, the formation energy of a SW defect tends to increase, but the corresponding bond length deviation amplitude decreases. It should be noted that size (tube radius) dependent properties of the intrinsic defects in periodic tubes are dominated by the curvature effect. However for a finite-length BNNT, curvature makes little difference for the defects at different sites. As it has been discussed, B−N bonds near the tube ends are elongated, expanding the tube and weakening the bond strengths to some extent. In this way, atoms near the ends are more susceptible to undergo SW-type transformation, but the system expanded already is less capable of taking the further structural transformation induced by the SW defect, which lead to a decreasing amplitude of the bond length deviation. Therefore, it is the weakening B−N bond near the tube ends that leads to above-mentioned evolution of SW defects. Another fact that needs to be addressed is SW defects marked with the same number (with the equal distance to their nearest ends) almost have the same bond length deviation, indicating that the discrepancy in their formation energies does not result from the structural deformation but should come from other origins.

3.3. Influence of Intrinsic Electric Polarization Field on the Defect Stability. Due to the heteropolar nature of the B−N bond and the 3-fold symmetry of the BN network, BN tubes can exhibit spontaneous electric polarization along the tube axis.[16] In principle, the electric polarization of BNNT can be influenced by defects because of their perturbations on electronic Hamiltonian and the breaking of 3-fold symmetry of an ideal tube. On the other hand, the existence of a macroscopic polarization field along the tube axis may affect physical quantities of defect systems as well.[32] In this subsection, the influence of intrinsic electric polarization field on the defect stability is under investigation.

In order to quantify the polarization field of a finite-length (8, 0) BNNT, its one-dimensional macroscopic average of the electrostatic potential is calculated. Based on the macroscopic average technique,[31] the planar average of electric potential is calculated as follows

$$\bar{f}(z) = \frac{1}{S}\int_S f(\vec{r})\,\mathrm{d}x\,\mathrm{d}y \tag{2}$$

where $f(\vec{r})$ is the magnitude of electricstatic potential at a given point $\vec{r}$, S is the area of the cross section perpendicular to the tube axis. Integrating the tube planar portion of the electric potential according to eq 3,[31] the average macroscopic electrostatic potential $\bar{\bar{f}}(z)$ can be obtained.

$$\bar{\bar{f}}(z) = \frac{1}{l}\int_{z-l/2}^{z+l/2} \bar{f}(z')\,\mathrm{d}z' \tag{3}$$

The slope of $\bar{\bar{f}}(z)$ is defined as the polarization field. Our calculated polarization field of a perfect (8, 0) BNNT is −0.013 eV/Å, which is well consistent with the reported result of previous publication.[33] Figure 5 plots the average planar and macroscopic electric potential distribution along the tube axis for the perfect BNNT. It is found there is a net polarization field (from N ends to B ends) existing in a perfect (8, 0) BNNT. Moreover, except for the tube end regions (gray areas in Figure 5), most of the tube is under a uniform electric field.

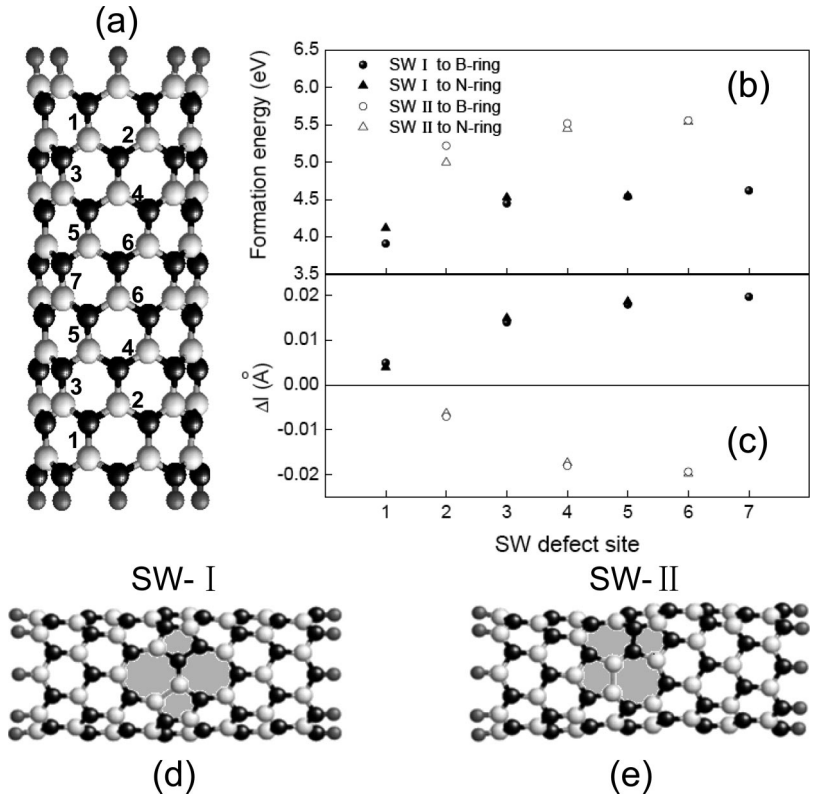

Figure 4. (a) Perfect (8, 0) BNNT, 1−7 indicate the sites where each B−N bond will be rotated to form a SW-I or SW-II defect. (b) The formation energy and (c) bond length deviation of B−N bond for the SW defect at each site. (d and e) The optimized structures where a B−N bond at sites 7 and 6 (closer to B-ring) is rotated. The SW defect region is marked as gray area and B−N bonds within this area are included for average B−N bond length calculation.

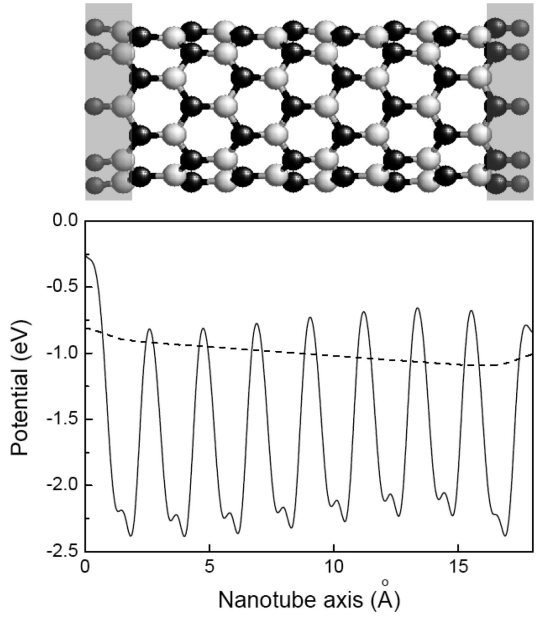

Figure 5. Schematic drawings of a perfect (8, 0) BNNT with finite length and corresponding average planar (solid line) and macroscopic (dashed line) electrostatic potential distribution along the nanotube axis.

When the intrinsic defect is moving along the tube axis, what effect will the electric field of the tube make on it? To answer this question, the average planar and macroscopic electrostatic potential of defective BNNT is studied. It is found that, as long as the defect is far away from the tube ends, the effect that the defect makes on the macroscopic electrostatic potential of the tube is little. Therefore, the electric field distribution of the defective tube is almost the same as that in the perfect tube. However, the intrinsic defect can induce a local change to planar electric potentials around the defect regions. Figure 6 plots the planar electrostatic potential distribution along the nanotube axis for the representative defective BNNT containing (a) V_N, (b) V_B, (c) SW-I, and (d) SW-II defects. The detailed analysis on electric potential of each defect is presented below.

Compared with the perfect BNNT, single vacancy makes the increase of electrostatic potential at the defect site. This fact together with the mulliken population analysis indicates that single vacancies are actually negative charged defect centers. As this negative charged point defect moves equidistantly from the B end (high electrostatic potential side) to N end (low potential side), under the polarization field of BN tube, the electrostatic potential around the vacancy defect is changed homogeneously. This field-induced electrostatic potential shift results in the regular change of total energy as well as Fermi level of the vacancy system. Exception occurs when an atom near the tube end is removed, where the electric potential around tube end is modified greatly, resulting in a significant change of tube polarization field and the Fermi level of the system as well. Therefore, the shift of the Fermi level for the single vacancy is primarily as a result of the change of the local electrostatic potential induced by the polarization field of BN tube.

Two kinds SW defects make the opposite change of local electric potential. Combining with the mulliken population results, it is indicated that SW-I and SW-II defects are two oppositely charged electric dipoles. Thus, as SW-I defects are favored to move toward the B end, SW-II will have the opposite preference. From this point of view, the formation energy discrepancy for the equidistant SW defects neighboring to B or

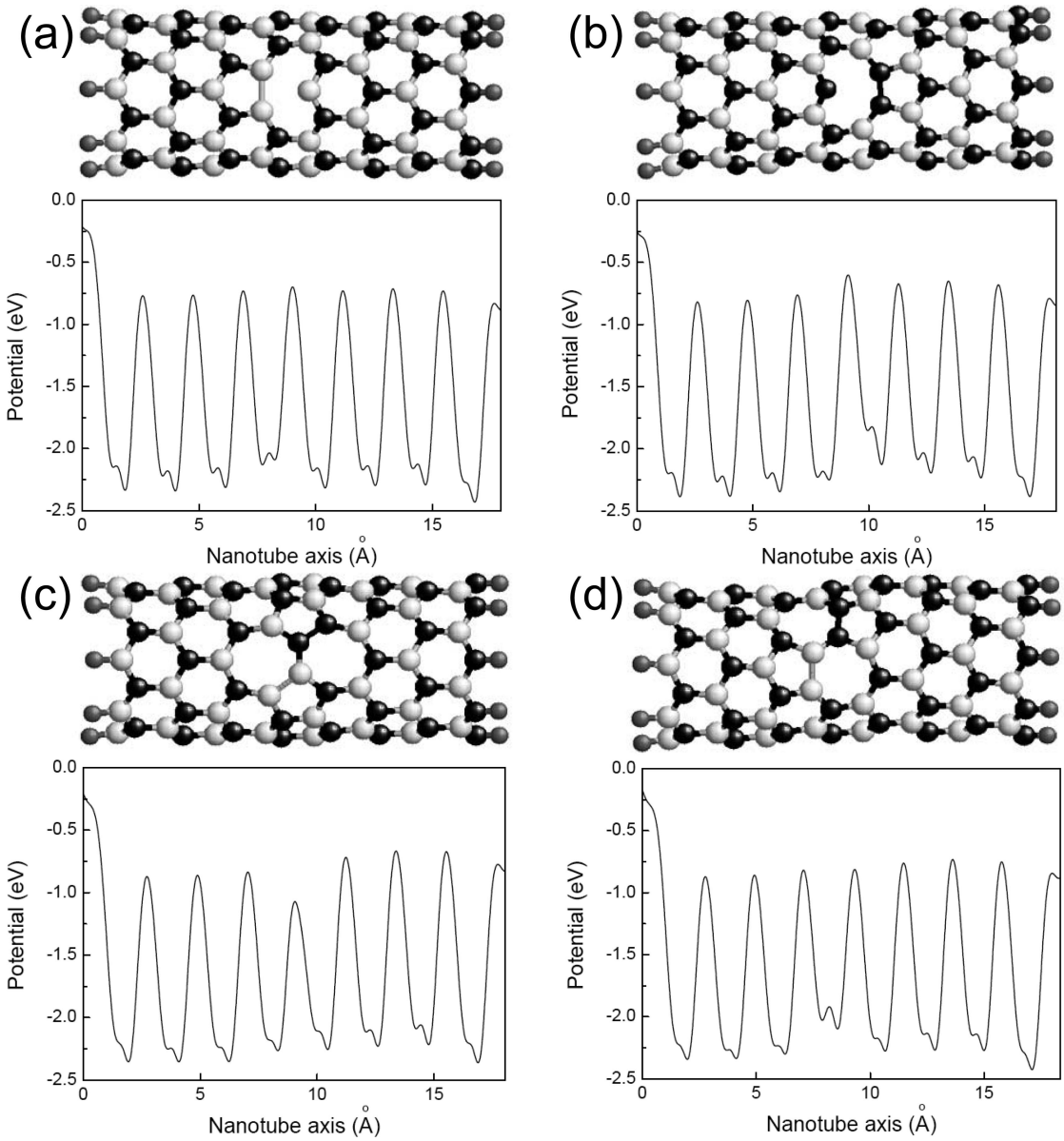

Figure 6. Schematic drawings of defective (8, 0) BNNTs with finite length and corresponding average planar electrostatic potential distribution along the nanotube axis for BNNT containing (a) V_N, (b) V_B, (c) SW-I, and (d) SW-II defects.

N ends can be ascribed to the change of electrostatic potential at defect sites. Therefore, it is concluded that intrinsic polarization field of BNNT can make the defects preferentially move toward the one specific tube end.

3.4. Experimental Consequences. The calculation above clearly reveals that in a finite-length tube, the stabilities of defects are enhanced as they become close to the tube ends. Two factors may act as "driving forces" for the energetic preference of defects: (i) the weakening of the B−N bond strength makes defects occur preferentially near the tube ends and (ii) the spontaneous electric field of polar BN tube makes the electrostatic potential difference for defects at the different sites along the tube axis. What experimental consequences can these theoretical findings lead to? In this subsection, this issue will be systematically investigated.

For a better illustration, we first review the similar theoretical study carried out on CNTs.[11] In CNTs, the stabilities of defects are enhanced greatly as they become closer to the tube open end. The large energy difference between the defects near and far from the tube end leads to the following scenario: at elevated temperatures, defects in a CNT can diffuse from the central part of the tube to the open end, where they can be healed by catalyst atoms. Because of the continuous migration of defects, there will exist a defect density gradient along the CNT. This kind of defect healing process may be crucial to understanding the growth mechanism of high-quality CNTs.

Despite the structural similarity between BNNTs and CNTs, the heteronuclear nature of the B−N bond is the origin of fundamental differences between the two systems. It is found that the defect healing behavior in a finite length BN tube is significantly different from that in CNT. For example, compared with their carbon analogues, corresponding defects in BNNTs have larger formation energies. The energy gain for defects diffusing from the tube center to the end are much smaller and the decrease of defect formation energy mainly occurs for the defects near the tube ends. Moreover, considering the relatively large energy barrier for defect migration in BN systems (the activation barrier for the SW defect in a (10, 0) BNNT is about 8 eV; in h-BN, V_N can not be thermally activated even at the melting point of h-BN),[14,15] the following experimental conse-

quences are expected in BN systems: BN tubes are more structurally stable against the thermal treatment damage. However, during their growing procedure, once the defects are formed on the tube wall (far from the open ends), the chance for them to migrate to the tube ends through thermal activation is rare. In other words, these defects are hard to be healed through self-migration to the open end but will remain on BNNT walls. In this way, resulting BNNT samples will be poor in quality. Therefore, the defect healing process in understanding the growth mechanism of CNTs can not properly work on BNNT systems.

In order to produce the BNNT samples of high quality, the synthetic techniques different from those used in CNTs preparation should be applied. To get rid of the residual defects, it is proposed that a relative low reactive temperature may be helpful, since the production yield of defects under thermal treatment damage can be greatly reduced at low temperature. Because the microscopic polarization field of polar BNNT makes the defects energeticly preferable toward one specific tube end. In the presence of external electric field, on the one hand, the growth direction of polar BN tubes can be well aligned to the electric field; on the other hand, the migrating ability of the defects along the tube axis can be greatly enhanced. Therefore, applying a strong electric field during the growth of BN tubes may be crucial to produce well aligned and high-quality BNNTs samples.

Recently, Geohegan et al. reported the successful synthesis of high-qulity BNNTs.[34] They prepared BNNT directly on the substrates at 600 °C by a plasma-enhanced pulsed-laser deposition (PE-PLD) technique, and a negative substrate bias voltage was applied to generate the reactive condition for growing BNNTs. Most importantly, their BNNT samples were constructed of high-order tubular structures and can be used without purification. These experimental results are well consistent with our theoretical simulations. Therefore, our work may provide a good theoretical support of this kind synthetic technique.

4. Conclusions

We have performed systematic ab initio calculations on finite-length perfect and defective (8, 0) BNNTs, containing V_B, V_N, or SW defects. It is found that stabilities of all intrinsic defects are enhanced, as they get close to the tube ends. Our findings indicate that two factors may provide the "driving forces" for defect energetic preference toward the tube ends: weakening the bond strength near the tube ends and the electric polarization field in polar BNNTs. Based on our simulations, we also discuss the potential experimental consequences and provide the theoretical support for one experimental method for the synthesis of high-quality BN tubes.

Acknowledgment. This work is financially supported by the Ministry of Science and Technology of China (NKBRSF-G1999064603), National Basic Research Program of China (2006CB922000 and 2009CB939901), National Science Foundation of China (Grant Nos. 10874161 and 10574115), and the Innovation Foundation of USTC for the Postgraduate (KD2007079). The HP-LHPC of USTC is acknowledged for computational support.

References and Notes

(1) Rubio, A.; Corkill, J. L.; Cohen, M. L. *Phys. Rev. B* **1994**, *49*, 5081.
(2) Chopra, N. G.; Luyken, R. J.; Cherrey, K.; Crespi, V. H.; Cohen, M. L.; Louie, S. G.; Zettl, A. *Science* **1995**, *269*, 966.
(3) Arenal, R.; Stéphan, O.; Kociak, M.; Taverna, D.; Loiseau, A.; Colliex, C. *Phys. Rev. Lett.* **2004**, *95*, 127601.
(4) Blase, X.; Rubio, A.; Louie, S. G.; Cohen, M. L. *Europhys. Lett.* **1994**, *28*, 335.
(5) Hernandez, E.; Goze, C.; Bernier, P.; Rubio, A. *Phys. Rev. Lett.* **1998**, *80*, 4502.
(6) Chang, C. W.; Fennimore, A. M.; Afanasiev, A.; Okawa, D.; Ikuno, T.; Garcia, H.; Li, D.; Majumdar, A.; Zettl, A. *Phys. Rev. Lett.* **2006**, *97*, 085901.
(7) Golberg, D.; Bai, X. D.; Mitome, M.; Tang, C. C.; Zhi, C. Y.; Bando, Y. *Acta Matter.* **2007**, *55*, 1293.
(8) Chen, Y.; Zhou, J.; Campell, S. J.; Caer, G. L. *Appl. Phys. Lett.* **2004**, *84*, 2430.
(9) Golberg, D.; Bando, Y.; Tang, C. C.; Zhi, C. Y. *Adv. Mater.* **2007**, *19*, 2413.
(10) Arenal, R.; Stephan, O.; Cochon, J. L.; Loiseau, A. *J. Am. Chem. Soc.* **2007**, *129*, 16183.
(11) Ding, F. *Phys. Rev. B* **2005**, *72*, 245409.
(12) Zobelli, A.; Ewels, C. P.; Gloter, A.; Seifert, G.; Stenphan, O.; Csillag, S.; Colliex, C. *Nano Lett.* **2006**, *6*, 1995.
(13) Bettinger, H. F.; Dumitric, T.; Scuseria, G. E.; Yakobson, B. I. *Phys. Rev. B* **2002**, *65*, R041406.
(14) Dumitric, T.; Bettinger, H. F.; Scuseria, G. E.; Yakobson, B. I. *Phys. Rev. B* **2003**, *68*, 085412.
(15) Zobelli, A.; Ewels, C. P.; Gloter, A.; Seifert, G. *Phys. Rev. B* **2007**, *75*, 094104.
(16) Mele, E. J.; Král, P. *Phys. Rev. Lett.* **2002**, *88*, 056803.
(17) Szwacki, N. G.; Sadrzadeh, A.; Yakobson, B. I. *Phys. Rev. Lett.* **2007**, *98*, 166804.
(18) Ordejón, P.; Artacho, E.; Soler, J. M. *Phys. Rev. B* **1996**, *53*, R10441.
(19) Sánchez-Portal, D.; Ordejón, P.; Artacho, E.; Soler, J. M. *Int. J. Quantum Chem.* **1997**, *65*, 453.
(20) Soler, J. M.; Artacho, E.; Gale, J. D.; García, A.; Junquera, J.; Ordejón, P.; Sánchez-Portal, D. *J. Phys.: Condens. Matter* **2002**, *14*, 2745.
(21) Troullier, N.; Martins, J. L. *Phys. Rev. B* **1991**, *43*, 1993.
(22) Kleinman, L.; Bylander, D. M. *Phys. Rev. Lett.* **1982**, *48*, 1425.
(23) Bylander, D. M.; Kleinman, L. *Phys. Rev. B* **1990**, *41*, 907.
(24) (a) Perdew, J. P.; Burke, K.; Ernzerhof, M. *Phys. Rev. Lett.* **1996**, *77*, 3865. (b) Perdew, J. P.; Burke, K.; Ernzerhof, M. *Phys. Rev. Lett.* **1997**, *78*, 1396.
(25) Sankey, O. F.; Niklewski, D. J. *Phys. Rev. B* **1989**, *40*, 3979.
(26) Press, W. H.; Flannery, B. P.; Teukolsky, S. A.; Vetterling, W. T. *New Numerical Recipes*; Cambridge University Press: New York, 1986.
(27) Gou, G. Y.; Pan, B. C.; Shi, L. *Phys. Rev. B* **2007**, *76*, 155414.
(28) Because of the unpreference of homoatomic B−B or N−N bond against the polar B-N bond, sp^3 hybridized defect structure exising in CNTs[11] is not available for BNNTs.
(29) Lu, A. J.; Pan, B. C. *Phys. Rev. Lett.* **2004**, *92*, 105504.
(30) Pan, B. C.; Yang, W. S.; Yang, J. L. *Phys. Rev. B* **2000**, *62*, 12652.
(31) Baldereschi, A.; Baroni, S.; Resta, R. *Phys. Rev. Lett.* **1988**, *61*, 734.
(32) Hu, S. L.; Li, Z. Y.; Zeng, X. C.; Yang, J. L. *J. Phys. Chem. C* **2008**, *112*, 8424.
(33) Zhang, J.; Loh, K. P.; Deng, M.; Sullivian, M. B.; Zhang, J. W.; Wu, P. *J. Appl. Phys.* **2006**, *99*, 104309.
(34) Wang, J.; Kayastha, V. K.; Yap, Y. K.; Fan, Z.; Lu, J. G.; Pan, Z.; Ivanov, I. N.; Puretzky, A. A.; Geohegan, D. B. *Nano Lett.* **2005**, *5*, 2528.

JP806530N